Available online at www.sciencedirect.com
SCIENCE DIRECT®
PERGAMON
International Journal of Heat and Mass Transfer 46 (2003) 2755–2771
International Journal of HEAT and MASS TRANSFER
www.elsevier.com/locate/ijhmt

Flow boiling heat transfer in two-phase micro-channel heat sinks—I. Experimental investigation and assessment of correlation methods

Weilin Qu, Issam Mudawar *

Boiling and Two-Phase Flow Laboratory, School of Mechanical Engineering, 1288 Mechanical Engineering Building, Purdue University, West Lafayette, IN 47907, USA

Received 27 September 2002; received in revised form 13 January 2003

Abstract

This paper is the first of a two-part study concerning measurement and prediction of saturated flow boiling heat transfer in a water-cooled micro-channel heat sink. In this paper, new experimental results are discussed which provide new physical insight into the unique nature of flow boiling in narrow rectangular micro-channels. The micro-channel heat sink contained 21 parallel channels having a 231×713 μm cross-section. Tests were performed with deionized water over a mass velocity range of 135–402 kg/m^2 s, inlet temperatures of 30 and 60 °C, and an outlet pressure of 1.17 bar. Results indicate an abrupt transition to annular flow near the point of zero thermodynamic equilibrium quality, and reveal the dominant heat transfer mechanism is forced convective boiling corresponding to annular flow. Contrary to macro-channel trends, the heat transfer coefficient is shown to decrease with increasing thermodynamic equilibrium quality. This unique trend is attributed to appreciable droplet entrainment at the onset of annular flow regime development, and the increase in mass flow rate of the annular film by droplet deposition downstream. Eleven previous empirical correlations are assessed and deemed unable to predict the correct trend of heat transfer coefficient with quality because of the unique nature of flow boiling in micro-channels, and the operating conditions of water-cooled micro-channel heat sinks falling outside the recommended application range for most correlations. Part II of this study will introduce a new annular flow model as an alternative approach to heat transfer coefficient prediction for micro-channels.

Keywords: Micro-channel; Flow boiling

1. Introduction

Two-phase micro-channel heat sinks are devices that feature flow boiling of a liquid coolant through parallel channels having a hydraulic diameter of 10–1000 μm. These devices are ideally suited for high-heat-flux dissipation from small surface areas in a broad range of emerging technologies. The combination of small flow passage area and flow boiling produce very high heat transfer coefficients with minimal flow rate and overall coolant inventory requirements, and provide better stream-wise temperature uniformity than single-phase micro-channel heat sinks [1–6].

Deployment of two-phase micro-channel technology requires a comprehensive fundamental understanding of virtually all hydrodynamic and thermal aspects of phase change in small channels. The ability to accurately predict pressure drop and flow boiling heat transfer for a given micro-channel geometry and operating conditions is of paramount importance to both the design and performance assessment of a micro-channel heat sink.

Because the interest in implementing these devices is fairly recent, brought about mostly by thermal

* Corresponding author. Tel.: +1-765-494-5705; fax: +1-765-494-0539.
E-mail address: mudawar@ecn.purdue.edu (I. Mudawar).

0017-9310/03/$ - see front matter © 2003 Elsevier Science Ltd. All rights reserved.
doi:10.1016/S0017-9310(03)00041-3

Nomenclature

A_t	planform area of heat sink top surface
Bo	boiling number
C	Martinelli–Chisholm constant
Co	convection number
c_P	specific heat at constant pressure
d_h	hydraulic diameter of micro-channel
E	coefficient in empirical correlations
F	coefficient in empirical correlations
f_f	friction factor based on local liquid flow
f_g	friction factor based on local vapor flow
Fr	Froude number
g	gravitational constant
G	mass velocity
H_{cell}	height of heat sink unit cell
H_{ch}	height of micro-channel
h_{fg}	latent heat of vaporization
h_{nb}	nucleate boiling heat transfer coefficient
h_{sp}	single-phase heat transfer coefficient
h_{tp}	two-phase heat transfer coefficient
H_{w1}	thickness of plastic cover plate
H_{w2}	distance from thermocouple to micro-channel bottom wall
k_f	thermal conductivity of water
k_s	thermal conductivity of copper heat sink
L	length of heat sink
L_{sat}	length of saturated region
L_{sub}	length of subcooled region
m	fin parameter
$\dot{m}$	mass flow rate
M	number of data points
M_W	molecular weight
MAE	mean absolute error
NN	Coefficient in empirical correlations
Nu_3, Nu_4	fully developed laminar Nusselt number for three and four wall heat transfer
P	pressure
$P_{p,out}$	pump exit pressure
P_r	reduced pressure
P_W	total power input
Pr	Prandtl number
ΔP_{sat}	change in vapor pressure corresponding to ΔT_{sat}
q''	heat flux
q''_{ch}	heat flux based on channel heated perimeter
q''_{eff}	heat flux based on heat sink top planform area
Re_f, Re_{fo}	Reynolds number based on local liquid flow and total flow as liquid
Re_g	Reynolds number based on local vapor flow
S	coefficient in empirical correlations
T	temperature
$T_{sat,tci}$	water saturation temperature at thermocouple location
T_{tci}	thermocouple reading ($i = 1$–4)
$T_{w,tci}$	channel bottom wall temperature at thermocouple location
ΔT_{sat}	channel wall superheat
ΔT_{sub}	liquid subcooling
v	specific volume
$\dot{V}$	volume flow rate
W	width of heat sink
W_{cell}	width of heat sink unit cell
W_{ch}	width of micro-channel
W_w	half-width of wall separating micro-channels
We	Weber number
x_e	thermodynamic equilibrium quality
X_{tt}	Martinelli parameter based on turbulent liquid—turbulent vapor flow
X_{vt}	Martinelli parameter based on laminar liquid—turbulent vapor flow
z	stream-wise location

Greek symbols

β	aspect ratio
η	fin efficiency
ϕ_f	two-phase frictional multiplier based on local liquid flow rate
μ	viscosity
σ	surface tension

Subscripts

0	zero thermodynamic equilibrium quality
cor	correlation
exp	experimental
f	liquid phase
g	vapor phase
in	inlet
out	outlet
pred	predicted
sat	saturated
sp	single-phase
sub	subcooled
tc*i*	thermocouple ($i = 1$–4)
tp	two-phase

management needs in computer and aerospace electronics, published studies on flow boiling in micro-channels are quite limited. However, there is an abundance of studies on flow boiling in mini-channels, which were

intended to aid in the design of compact heat exchangers. The hydraulic diameter for mini-channels is typically on the order of a few millimeters, which is several times larger than those found in micro-channel heat sinks. Nonetheless, the findings from mini-channel studies are useful at pointing out fundamental differences in flow boiling behavior as hydraulic diameter is reduced from macro-scale (several centimeters) to the mini-channel scale, and progressively to micro-channel.

Some of the more relevant studies on flow boiling in mini/micro-channels are summarized in Table 1. Those studies clearly point to a departure in small channel boiling behavior from that of macro channels, and cite appreciable deviations in predictions of popular macro-channel heat transfer correlations from mini/micro-channel data. For example, several studies point to a decreasing heat transfer coefficient with increasing vapor quality in the saturated flow boiling region, which is contradictory to macro-channel trends [10,12–14,20]. Aside from general consensus over these deviations, the understanding of flow boiling in mini/micro-channels remains illusive. Furthermore, most mini/micro-channel studies use refrigerants as coolant, and the number of published studies using water is very limited. This is especially concerning since water is becoming the coolant of choice for many high-heat-flux cooling situations (e.g., lasers and fusion reactor blankets) because its thermal transport properties are far superior to those of all known refrigerants.

This two-part study will explore the flow boiling heat transfer characteristics of water in micro-channel heat sinks. The primary objectives of this study are to conduct a thorough experimental investigation of the heat transfer characteristics, assess the suitability of previous empirical correlations, and develop flow-pattern-based predictive tools for micro-channel heat sink design. In this Part I of the study, the findings from the experimental investigation are discussed, and fundamental differences from macro-channel results identified. This is followed by assessment of six popular macro-channel correlations and five correlations specifically developed for mini/micro-channels, through comparison between correlation predictions and the present experimental data. In the part II of this study [21], an annular flow model is developed to describe flow boiling in the saturated region of the micro-channel heat sink, which provides an alternative theoretical means to predicting the heat transfer coefficient.

2. Experimental apparatus

2.1. Flow loop

The experimental apparatus employed in this study was used in a previous study by the authors involving single-phase micro-channel heat sinks [22]. Fig. 1 shows a schematic of the flow loop that was configured to supply deionized water to the micro-channel heat sink test module at desire operating conditions. A reservoir served as both a constant pressure reference point for the loop and a deaeration chamber. The water was circulated through the loop using a variable speed gear pump. The test module fluid was first routed through a filter to remove solid particles that may cause blockage of the micro-channels. The water then entered one of two rotameters for flow rate measurement. Exiting the rotameter, the water passed through a heat exchanger, which was connected to a constant temperature bath, to bring the water to the desired module inlet temperature. The spent fluid exiting the test module passed through a water-cooled condenser to condense any vapor before the water returned to the reservoir.

2.2. Test module

Fig. 2 illustrates the construction of the test module, which was composed of an oxygen-free copper micro-channel heat sink, a G-7 fiberglass housing, a transparent polycarbonate plastic (Lexan) cover plate, and twelve cartridge heaters. A cross-sectional view of the assembled test module is shown in Fig. 3. The planform (top) surface of the heat sink measured 1.0 cm in width and 4.48 cm in length. Twenty-one rectangular 231 μm wide and 712 μm deep micro-slots were formed within the 1-cm width of the top surface. Below the heat sink top surface, four Type-K thermocouples were inserted along the center plane to measure the heat sink's stream-wise temperature distribution; they are indicated in Fig. 2 as tc1 to tc4 from upstream to downstream. Further below was a small protruding platform around the periphery of the heat sink to make certain the top surface of the heat sink was flush with the top surface of the housing as illustrated in Fig. 3. Three narrow deep slots were cut from the bottom surface up through most of the heat sink's height to reduce axial heat conduction within the heat sink. Twelve holes were drilled into the heat sink bottom surface to accommodate the cartridge heaters. These heaters were powered by a 0–110 VAC variac and their total electrical power was measured by a precision wattmeter.

The housing contained plenums both upstream and downstream of the micro-channels to ensure even flow distribution. Located in the plenums were two absolute pressure transducers and two Type-K thermocouples for inlet and outlet pressure and temperature measurement, respectively. The cover plate was bolted atop the housing to form the micro-channels. The transparent cover plate facilitated direct visual access to the two-phase flow in the micro-channels. After the test module was assembled, multiple layers of ceramic fiber were wrapped around the heat sink to reduce heat loss to the ambient.

Table 1
Summary of previous investigations on flow boiling heat transfer in mini/micro-channels

Author(s) [reference] (year)	Channel geometry and size	Cooling fluid	Parameter range	Dominant heat transfer mechanism	Remarks
Lazarek and Black [7] (1982)	Single tube 3.15 mm i.d.	R-113	$G = 125$–750 kg/m^2 s $P = 1.3$–4.1 bar $q'' = 1.4$–38 W/cm^2 $\Delta T_{sub,in} = 3$–73 °C	Nucleate boiling	The heat transfer coefficient was independent of x_e for $x_e \geqslant 0$. Predictions from Chen [8] and Shah [9] correlations were compared with experimental data. Shah correlation [9] showed reasonable agreement. An empirical correlation was proposed, where the two-phase Nusselt number was correlated to the boiling number and the liquid Reynolds number
Wambsganss et al. [10] (1993)	Single tube 2.92 mm i.d.	R-113	$G = 50$–300 kg/m^2 s $P_{out} = 1.24$–1.6 bar $q'' = 0.88$–9.075 W/cm^2 $x_e = 0$–0.9 $T_{in} = 20$–50 °C	Nucleate boiling	The heat transfer coefficient decreased slightly with increasing x_e for $x_e \geqslant 0$. Predictions from 10 empirical correlations were compared with experimental data. The Lazarek and Black correlation [7] showed the best agreement
Tran et al. [11] (1996)	Single tube 2.46 mm i.d. Single rectangular channel 4.06×1.7 mm	R-12	$G = 44$–832 kg/m^2 s $P = 5.1, 8.2$ bar $q'' = 0.36$–12.9 W/cm^2 $x_e = 0$–0.94	Nucleate boiling at wall superheats >2.75 °C, forced convective boiling at wall superheats <2.75 °C	The heat transfer coefficient was independent of x_e for $x_e \geqslant 0.2$. Predictions of three large tube correlations were unsuccessful at predicting the data. An empirical correlation was proposed, where the heat transfer coefficient was correlated to the boiling number, Weber number, and liquid to vapor density ratio. No significant geometrical effect was found between the circular tube and rectangular channel
Kew and Cornwell [12] (1997)	Single tubes 1.39–3.69 mm i.d.	R-141b		Nucleate boiling, confined bubble boiling, convective boiling, partial dry-out	For larger tubes (2.87 and 3.69 mm i.d.), the heat transfer coefficient decreased slightly or remained constant with increasing x_e for $x_e \leqslant 0.2$, but increased for $x_e \geqslant 0.2$. For the smaller tube (1.39 mm i.d.), the heat transfer coefficient increased with increasing x_e at low G for $x_e \geqslant 0$, but decreased rapidly at high G for $x_e \geqslant 0$. Predictions from six empirical correlations were compared with experimental data; none showed good agreement
Ravigururajan [13] (1998)	54 parallel rectangular channels 0.27×1.0 mm	R-124	$\dot{V} = 35$–300 ml/min $P_W = 20$–300 W $x_e = 0$–0.5		The heat transfer coefficient decreased monotonically with increasing x_e and increasing wall superheat for $x_e \geqslant 0$
Yan and Lin [14] (1998)	28 parallel tubes 2 mm i.d.	R-134a	$G = 50$–200 kg/m^2 s $q'' = 0.5$–2 W/cm^2		The heat transfer coefficient decreased with increasing x_e for $x_e \geqslant 0$ for several test conditions, and was affected by heat flux, fluid saturation temperature, and mass velocity. An empirical correlation was proposed, which had a form similar to that of the Kandlikar correlation [15]

Bao et al. [16] (2000)	Single tube 1.95 mm i.d.	R-12, HCFC 123	$G = 50$–1800 kg/m^2 s $P = 2$–5 bar $q'' = 0.5$–20 W/cm^2 $x_e = 0$–0.9	Nucleate boiling	The heat transfer coefficient was independent of x_e for $x_e \geqslant 0$. Predictions from ten empirical correlations were compared with experimental data. The Cooper pool boiling correlation [17] showed reasonable predictions
Lee and Lee [18] (2001)	3 single rectangular channels 20 mm wide 0.4, 2 and 2 mm deep	R-113	$G = 50$–200 kg/m^2 s $q'' = 0$–1.5 W/cm^2 $x_e = 0.15$–0.75	Forced convective boiling	The heat transfer coefficient increased with increasing x_e for $x_e \geqslant 0.15$. A correlation was developed based on an annular flow model for low G ($Re_f \leqslant 200$), where the heat transfer coefficient was correlated to the single-phase heat transfer coefficient, channel aspect ratio, and modified two-phase frictional multiplier. Kandlikar correlation [15] was recommended for high G ($Re_f > 200$)
Yu et al. [19] (2002)	Single tube 2.98 mm i.d.	Water	$G = 50$–200 kg/m^2 s $P = 2$ bar T_{in} = ambient to 80 °C	Nucleate boiling at wall superheats <8 °C, transition boiling at wall superheats >8 °C	Predictions of Chen correlation [8] were compared with experimental data. The predicted results were well centered but showed relatively large scatter. An empirical correlation was proposed for the nucleate boiling region, where the heat transfer coefficient was correlated to the boiling number, Weber number, and liquid to vapor density ratio
Warrier et al. [20] (2002)	5 parallel rectangular channels 0.75 mm hydraulic diameter	FC-84	$G = 557$–1600 kg/m^2 s $q'' = 0$–5.99 W/cm^2 $T_{in} = 26, 40, 60$ °C		The heat transfer coefficient decreased monotonically with increasing x_e for $x_e \geqslant 0$. Predictions of six empirical correlations were compared with experimental data; none showed good agreement. An empirical correlation was proposed for saturated flow boiling heat transfer, where the heat transfer coefficient was correlated to the single-phase heat transfer coefficient, boiling number and vapor quality

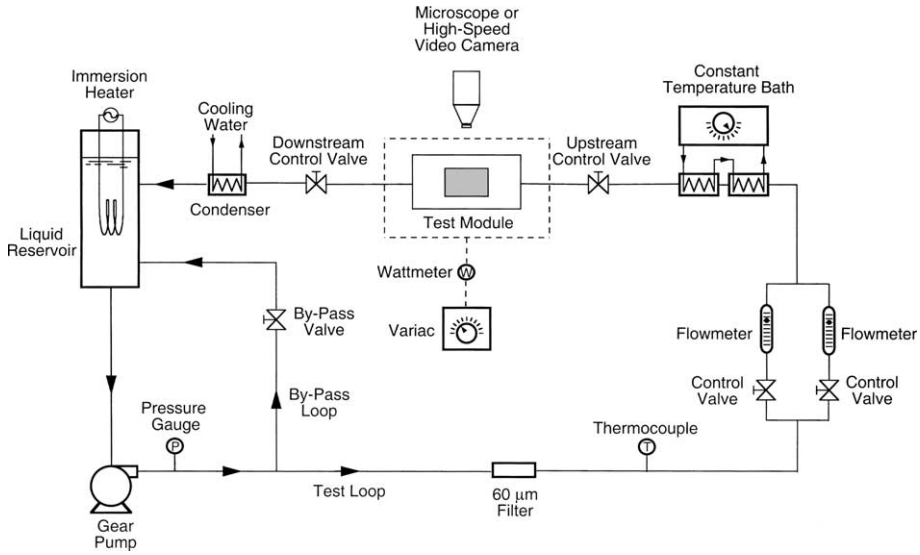

Fig. 1. Schematic of flow loop.

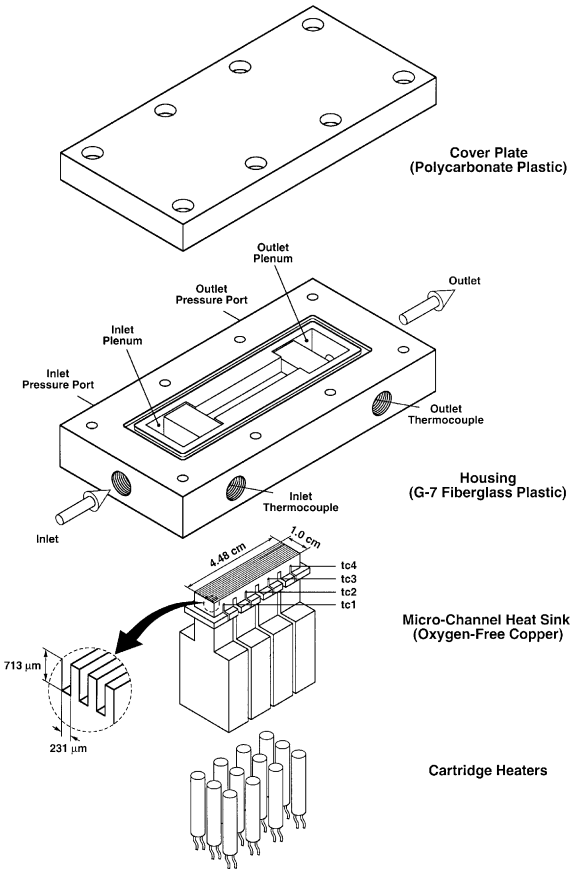

Fig. 2. Test module construction.

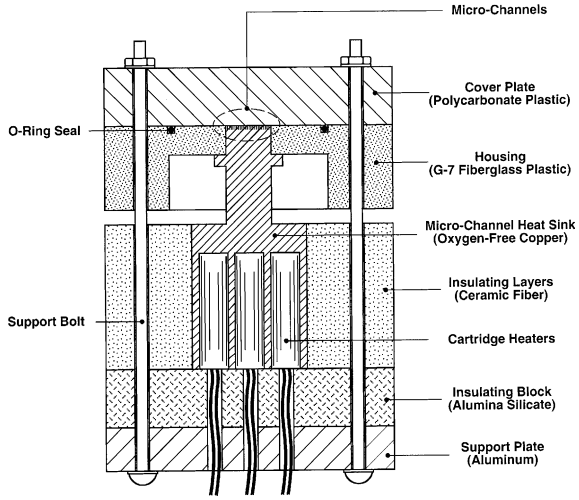

Fig. 3. Cross-section of test module assembly.

The wattmeter used to measure the electrical power input to the cartridge heaters had an accuracy of 0.5%. Error associated with the thermocouple readings was smaller than ± 0.3 °C, and measurement uncertainty of the pressure transducers and flow meters was better than 3.5% and 4%, respectively.

Prior to performing flow boiling experiments, a series of single-phase tests were conducted within the same flow rate range. Comparison between electrical power input and water enthalpy increase during the single-phase tests proved heat loss was less than 4%. All heat

Table 2
Operating conditions for present study

Coolant	Inlet temperature, T_{in} (°C)	Mass velocity, G (kg/m^2 s)	Outlet pressure, P_{out} (bar)	Pump exit pressure, $P_{p,out}$ (bar)
Deionized water	30.0	135–400	1.17	2.0
	60.0	135–402	1.17	2.0

flux data presented in this study were therefore based on the measured electrical power input.

2.3. Experimental procedure

Prior to conducting a test, the water in the reservoir was deaerated by vigorous boiling for about one hour to force any dissolved gases to escape to the ambient. Afterwards, the flow loop components were adjusted to yield the desired module inlet temperature, T_{in}, mass velocity, G, outlet pressure, P_{out}, and pump exit pressure, $P_{p,out}$, as indicated in Table 2. The mass velocity G was determined from measured mass flow rate, $\dot{m}$. Using the throttling valve situated upstream of the test module, the pump exit pressure, $P_{p,out}$, was elevated to 2.0 bar to prevent flow oscillations. Two-phase hydrodynamic instabilities encountered during flow boiling in micro-channel heat sinks, and means of preventing those instabilities have been addressed in a previous study by the authors [23].

After the flow became stable, the heater power was adjusted to a level below incipient boiling. The power was then increased in small increments as the flow loop components were constantly adjusted to maintain the desired operating conditions. Once steady-state conditions prevailed, the inlet and outlet pressures, P_{in} and P_{out}, inlet and outlet temperatures, T_{in} and T_{out}, and heat sink temperatures, T_{tc1} to T_{tc4}, were all recorded at 0.5 s intervals for 5 min. In the present study, the input heat flux level is represented by an effective heat flux,

$$q''_{eff} = \frac{P_W}{A_t}, \tag{1}$$

based on the top planform area, $A_t = 1.0 \times 4.48$ cm^2, of the heat sink.

Each test was terminated when the thermodynamic equilibrium quality, x_e, reached about 0.2 at the channel exit.

2.4. Data reduction

As indicated in Table 2, water was supplied into the heat sink in a subcooled state ($T_{in} < T_{sat}$) for all test conditions. The micro-channels can therefore be divided into two regions: an upstream subcooled inlet region and a downstream saturated region; the location of zero thermodynamic equilibrium quality ($x_e = 0$) serves as a dividing point between the two regions. The length of the two regions can be evaluated from

$$L_{sub} = \frac{\dot{m} c_{P,f}(T_{sat,0} - T_{in})}{q''_{eff} W} \tag{2}$$

and

$$L_{sat} = L - L_{sub}, \tag{3}$$

where $T_{sat,0}$ is the saturation temperature at the location where $x_e = 0$. In the present study, $T_{sat,0}$ is evaluated using the measured inlet pressure, P_{in}, assuming pressure drop across the subcooled region is small. Eqs. (2) and (3) indicate as the heat flux increases for a constant mass flow rate, L_{sat} increases at the expense of L_{sub}.

Determination of the local flow boiling heat transfer coefficient requires knowledge of local fluid temperature, micro-channel wall temperature, and heat flux. Since subcooled boiling may occur upstream of the point of zero thermodynamic equilibrium quality, the heat transfer coefficient can be accurately evaluated only at stream-wise locations which are in the saturated region ($x_e \geqslant 0$), and where the heat sink temperatures were measured by thermocouples tc1 to tc4. For the present test conditions, the two upstream thermocouples were mostly within the subcooled region. Therefore, only saturated heat transfer coefficient results that were obtained at locations z_{tc3} and z_{tc4} of the two downstream thermocouples are of interest.

To evaluate the boiling heat transfer coefficient, a two-dimensional unit cell comprised of a single micro-channel and surrounding solid is examined at axial locations where the heat sink thermocouples are situated. The unit cell is illustrated in Fig. 4 and its dimensions are given in Table 3. Unlike circular tubes that are employed in most flow boiling studies, the present configuration is complicated by nonuniformity of heat flux and wall superheat around the perimeter of the rectangular micro-channel. While it may be desirable to evaluate the distribution of heat transfer coefficient, such an endeavor requires wall temperature measurements along the entire perimeter. Such measurements were not possible because of the extreme difficulty in fabricating multiple surface micro-sensors that do not interfere with the boiling process in a micro-channel. Therefore, a mean heat transfer coefficient, h_{tp}, averaged over the heated perimeter of the micro-channel, was obtained using the fin analysis method. This is a technique that

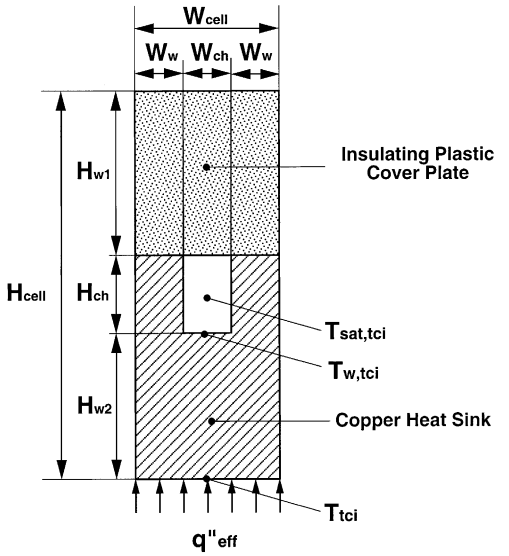

Fig. 4. Two-dimensional micro-channel heat sink unit cell.

Table 3
Dimensions of micro-channel heat sink unit cell

W_w (μm)	W_{ch} (μm)	H_{w1} (μm)	H_{ch} (μm)	H_{w2} (μm)
118	231	12,700	713	2462

was employed by previous investigators to determine the flow boiling heat transfer coefficient in narrow channels with serrated fins [24] and with offset strip fins [25,26]. A comprehensive discussion on the application of the fin analysis method to evaluate the mean heat transfer coefficient for single-phase water flow in micro-channel heat sinks is available in a previous study by the authors [27]. Basically, this method models the solid walls separating micro-channels as thin fins and adopts specific approximations such as one-dimensional heat diffusion. It also employs a single mean convective heat transfer coefficient value along the entire heated perimeter.

Applying the fin analysis method to the unit cell shown in Fig. 4 yields the following energy balance

$$q''_{\text{eff}} W_{\text{cell}} = h_{\text{tp}}(T_{\text{w,tc}i} - T_{\text{sat,tc}i})(W_{\text{ch}} + 2\eta H_{\text{ch}}). \quad (4)$$

The left-hand side of Eq. (4) represents heat input to the unit cell, and the right-hand side the rate of heat removal by flow boiling from the channel walls, neglecting the miniscule heat loss from the insulating plastic cover plate. The thin fin approximation is applied to the channel side walls by introducing the fin efficiency

$$\eta = \frac{\tanh(mH_{\text{ch}})}{mH_{\text{ch}}}, \quad (5)$$

where m is the fin parameter,

$$m = \sqrt{\frac{h_{\text{tp}}}{k_{\text{s}} W_{\text{w}}}}. \quad (6)$$

In Eq. (4), $T_{\text{w,tc}i}$ represents the temperature of the channel bottom wall, which can be calculated by assuming one-dimensional heat diffusion.

$$T_{\text{w,tc}i} = T_{\text{tc}i} - \frac{q''_{\text{eff}} H_{\text{w2}}}{k_{\text{s}}}. \quad (7)$$

$T_{\text{sat,tc}i}$ in Eq. (4) is based on the local pressure. The pressure at the location of $x_e = 0$ is set equal to measured P_{in}, and the pressure at the channel outlet to measured P_{out}. Linear interpolation is employed to determine the pressure at the thermocouple locations, from which the saturation temperature $T_{\text{sat,tc}i}$ is determined. This procedure for estimating the saturation temperature is justified by the relatively small pressure drop (<0.2 bar) associated with the present experiments.

Once $T_{\text{w,tc}i}$ and $T_{\text{sat,tc}i}$ are determined, the value of mean flow boiling heat transfer coefficient, h_{tp}, can be readily determined from Eq. (4).

3. Results and discussion

3.1. Boiling curves

Fig. 5 shows typical boiling curves obtained at the four thermocouple locations for $T_{\text{in}} = 60$ °C and $G = 255$ kg/m^2 s. In these curves, q''_{eff} is plotted versus the difference between channel bottom wall temperature $T_{\text{w,tc}i}$ and T_{in}, where $T_{\text{w,tc}i}$ is obtained from Eq. (7). At low heat fluxes, the slopes of all boiling curves are fairly constant, indicative of single-phase heat transfer. As the

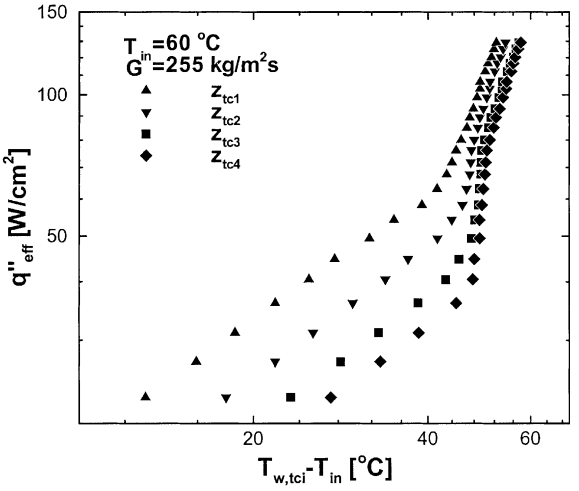

Fig. 5. Boiling curves at z_{tc1} to z_{tc4} for $T_{\text{in}} = 60$ °C and $G = 255$ kg/m^2 s.

heat flux increases, the slope of the boiling curve at z_{tc4} begins to increase first, indicating flow boiling had commenced at that location. With further increases in heat flux, the increase in slope associated with the initiation of flow boiling is detected at upstream thermocouple locations as well, evidence of upstream propagation of the boiling front.

3.2. Saturated flow boiling heat transfer coefficient

Fig. 6(a) and (b) shows the variation of the saturated flow boiling heat transfer coefficient h_{tp} at the axial location of thermocouple tc4 with thermodynamic equilibrium quality x_e for inlet temperatures of 30 and 60 °C, respectively. Five mass velocities within the range of 135–402 kg/m^2 s were tested for each inlet temperature. The overall range of h_{tp}, 20–45 kW/m^2 °C, is fairly similar to that measured by Yu et al. [19], 10–50 kW/m^2 °C; the latter is for water flow boiling in a single mini-tube.

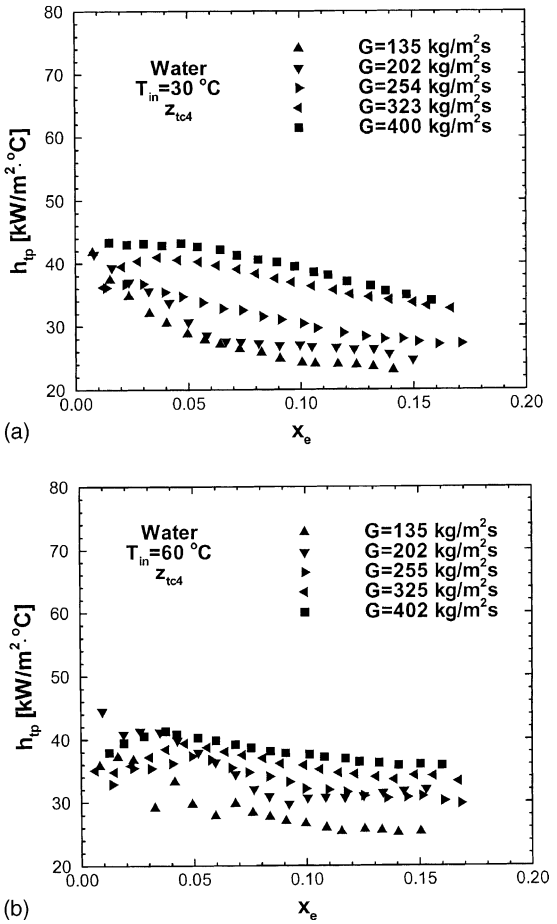

Fig. 6. Saturated flow boiling heat transfer coefficient versus thermodynamic equilibrium quality at z_{tc4} for (a) $T_{in} = 30$ °C and (b) $T_{in} = 60$ °C.

It is widely accepted that saturated flow boiling in channels is governed by two mechanisms: nucleate boiling and forced convection boiling [28]. In the nucleate boiling dominant region, liquid near the heated channel wall is superheated to a sufficient degree to sustain the nucleation and growth of vapor bubbles. The heat transfer coefficient in this region is dependent upon heat flux, but generally far less sensitive to mass velocity and vapor quality. The nucleate boiling region is normally associated with the bubbly and slug flow patterns, and the forced convection boiling region with the annular flow pattern. In the forced convection boiling dominant region, large h_{tp} causes suppression of bubble nucleation along the heated wall, so the heat is transferred mainly by single-phase convection through the thin annular liquid film and carried away by evaporation at the liquid–vapor interface. The heat transfer coefficient in this region is dependent upon coolant mass velocity and vapor quality, but fairly independent of heat flux.

It follows from the above discussion that the measured variation of saturated flow boiling heat transfer coefficient with mass velocity, vapor quality, and heat flux, coupled with the observed two-phase flow pattern, constitute the physical basis for identifying the dominant heat transfer mechanism in a micro-channel. As indicated in Fig. 6(a) and (b), h_{tp} increases appreciably with increasing G for a given x_e and decreases with increasing x_e for a constant G. The latter trend is unique to mini/micro-channel flow boiling as will be discussed in a later section.

To fully understand the heat transfer mechanism, the influence of heat flux on h_{tp} should also to be addressed. Unfortunately, this effect cannot be decoupled from that of x_e due to the limited number of heat sink temperature measurements performed along the stream-wise direction. x_e at a given location increases with increasing input heat flux q''_{eff} when G is kept constant. The observed trend of decreasing h_{tp} with increasing x_e, Fig. 6(a) and (b), implies h_{tp} may also decrease with increasing q''_{eff}. This trend does not support the nucleate boiling mechanism, which is normally associated with a significant increase in h_{tp} with increasing q''_{eff} due to intensification of bubble nucleation along the channel wall. Furthermore, previous visualization studies of flow boiling in micro-channels reveal the annular flow pattern is dominant for moderate to high heat fluxes [4,5,23]. All these facts lead to the conclusion that forced convection boiling is the dominant mechanism for the saturated region in the present micro-channel heat sink.

As shown in Table 1, a few investigators indicated the dominant heat transfer mechanism for mini-channels is nucleate boiling, based largely on a strong dependence of the heat transfer coefficient on heat flux and a weaker dependence on G and x_e [7,10,11,16]. The apparent discrepancy between these findings and those of the present

study may be attributed to several fundamental differences between the earlier studies and the present. First, the dominant nucleate boiling mechanism in mini-channels was attributed by Lazarek and Black [7] and Wambsganss et al. [10], who used R-113 as working fluid, to high boiling number, 2.3×10^{-4} to 7.6×10^{-3} and 5.0×10^{-4} to 2.5×10^{-3}, respectively. A boiling number, *Bo*, for the present rectangular micro-channel geometry can be defined relative to mean heat flux along the heated perimeter,

$$Bo = \frac{q''_{ch}}{Gh_{fg}}, \tag{8}$$

where

$$q''_{ch} = \frac{q''_{eff} W_{cell}}{W_{ch} + 2H_{ch}}. \tag{9}$$

Eq. (8) yields a boiling number range for the present study of 2.2×10^{-4} to 7.8×10^{-4}, which is significantly lower than the previous two studies.

Second, flow boiling of water in micro-channels is drastically different from that of refrigerants. A recent study by Mukherjee and Mudawar [29] demonstrated fundamental differences in flow boiling behavior in micro-channels between water and FC-72; the latter is a fluorochemical coolant with thermophysical properties fairly similar to those of R-113. They pointed out that the low surface tension and small contact angle of fluorochemicals produce bubble departure diameters that are one to two orders of magnitude smaller than those for water. This means fluorochemicals (including most refrigerants) may sustain nucleate boiling over a significant portion of the micro-channel length, including the high vapor quality region, while vapor bubbles in water will grow to engulf much of the channel's cross-section and trigger a rapid transition to annular flow near the axial location of $x_e = 0$.

As mentioned in the previous section, the present data point to a decreasing heat transfer coefficient with increasing x_e. This trend is consistent with several previous experimental studies [10,12–14,20]. Ravigururajan [13] attributed this phenomenon to possible blockage of the channel width (for a rectangular channel) by vapor bubbles. Kew and Cornwell [12] and Warrier et al. [20], on the other hand, explained this trend by local dry-out beneath the vapor bubbles.

Alternatively, this trend may be explained by the unique behavior of annular flow in micro-channels. In annular flow, the vapor flows along the core of the channel, while liquid is comprised of two portions: the annular film along the channel wall, and droplets that are entrained in the vapor core. As indicated above, flow boiling of water in micro-channels features abrupt transition to annular flow and the absence of bubbly flow at moderate to high heat fluxes [4,5,23]. It is therefore possible that a large amount of liquid droplets are broken off into the vapor core at the onset of annular flow development. The deposition of droplets upon the annular liquid film increases the film thickness in the stream-wise direction, resulting in the observed trend of decreasing h_{tp} with increasing x_e. In part II of this study [21], this important postulation will be incorporated into an annular flow model to predict the saturated flow boiling heat transfer coefficient.

This and other peculiarities of flow boiling in micro-channel emphasize the need to develop new tools to predict micro-channel heat sink thermal performance. However, before such tools can be developed, it is prudent to assess the feasibility of previous correlations in predicting the present heat transfer coefficient results. The next section will explore the suitability of such correlations by differentiating between those developed for conventional macro-channels from those for mini- and micro-channels, due to the obvious differences in boiling behavior resulting from channel size.

4. Assessment of empirical correlations

4.1. Rationale

Eleven empirical correlations for the saturated flow boiling heat transfer coefficient in macro channels are selected and summarized in Table 4. It should be noted that most such correlations were developed for circular tubes. Application of these correlations to rectangular channels is fairly straightforward where all four walls transfer heat to the coolant. However, the micro-channel heat sink used in the present study, like most practical heat sinks, involve heat transfer along only three walls, since the channel top wall is typically adiabatic. To accommodate the difference, a correction factor is introduced.

$$h_{tp} = h_{tp,cor} \frac{Nu_3}{Nu_4}, \tag{10}$$

where $h_{tp,cor}$ is the heat transfer coefficient evaluated directly from a correlation, and Nu_3 and Nu_4 are the single-phase fully developed laminar Nusselt numbers for the conditions of three and four wall heat transfer, respectively [35,36],

$$Nu_3 = 8.235(1 - 1.883\beta + 3.767\beta^2 - 5.814\beta^3 + 5.361\beta^4 - 2.0\beta^5), \tag{11}$$

and

$$Nu_4 = 8.235(1 - 2.042\beta + 3.085\beta^2 - 2.477\beta^3 + 1.058\beta^4 - 0.186\beta^5). \tag{12}$$

This correction approach was used by Phillips [37] and Choquette et al. [38] to evaluate the mean heat transfer

Table 4
Flow boiling heat transfer correlations

Correlation	Reference	Heat transfer coefficient, h_{tp}	MAE (%)
1	Chen [8] (1966), Edelstein et al. [30] (1984)	$h_{tp} = \frac{Nu_3}{Nu_4}(Eh_{sp} + Sh_{nb})$ $h_{sp} = 0.023(Re_f)^{0.8}(Pr_f)^{0.4}\frac{k_f}{d_h},\ h_{nb} = 0.00122\left(\frac{k_f^{0.79}c_{p,f}^{0.45}v_g^{0.24}}{\sigma^{0.5}\mu_f^{0.29}h_{fg}^{0.24}v_f^{0.49}}\right)\Delta T_{sat}^{0.24}\Delta P_{sat}^{0.75}$ $E = \left(1+\frac{1}{X_{tt}^{0.5}}\right)^{1.78},\ S = 0.9622 - 0.5822\left[\tan^{-1}\left(\frac{Re_f E^{1.25}}{6.18\times10^4}\right)\right]$ $Re_f = \frac{G(1-x_e)d_h}{\mu_f},\ Pr_f = \frac{c_{p,f}\mu_f}{k_f},\ X_{tt} = \left(\frac{1-x_e}{x_e}\right)^{0.9}\left(\frac{v_f}{v_g}\right)^{0.5}\left(\frac{\mu_f}{\mu_g}\right)^{0.1}$	43.9
2	Shah [9,31] (1976,1982)	$h_{tp} = \frac{Nu_3}{Nu_4}\max(E,S)h_{sp}$ $h_{sp} = 0.023(Re_f)^{0.8}(Pr_f)^{0.4}\frac{k_f}{d_h}$ For $NN > 1.0,\ S = 1.8/NN^{0.8},\ E = 230Bo^{0.5}(Bo > 3\times10^{-5})$ or $E = 1 + 46Bo^{0.5}(Bo < 3\times10^{-5})$ For $0.1 < NN \leqslant 1.0,\ S = 1.8/NN^{0.8},\ E = FBo^{0.5}\exp(2.74NN^{-0.1})$ For $NN \leqslant 0.1,\ S = 1.8/NN^{0.8},\ E = FBo^{0.5}\exp(2.47NN^{-0.15})$ $F = 14.7\ (Bo \geqslant 11\times10^{-4})$ or $F = 15.43(Bo < 11\times10^{-4})$ $NN = Co\ (Fr_f \geqslant 0.04)$ or $NN = 0.38Fr_f^{-0.3}Co\ (Fr_f < 0.04)$ $Co = \left(\frac{1-x_e}{x_e}\right)^{0.8}\left(\frac{v_f}{v_g}\right)^{0.5},\ Fr_f = \frac{v_f^2G^2}{gd_h}$	53.7
3	Gungor and Winterton [32] (1986)	$h_{tp} = \frac{Nu_3}{Nu_4}(Eh_{sp} + Sh_{nb})$ $h_{sp} = 0.023(Re_f)^{0.8}(Pr_f)^{0.4}\frac{k_f}{d_h},\ E = 1 + 24000Bo^{1.16} + 1.37\left(\frac{1}{X_{tt}}\right)^{0.86}$ $h_{nb} = 55P_r^{0.12}(-\log_{10}(P_r))^{-0.55}M_W^{-0.5}q''^{0.67}_{ch},\ S = (1 + 1.15\times10^{-6}E^2Re_f^{1.17})^{-1}$ If $Fr_f \leqslant 0.05$, replace E by $EFr_f^{0.1-2Fr_f}$ and S by $SFr_f^{0.5}$, respectively	50.1
4	Kandlikar [15] (1990)	$h_{tp} = \frac{Nu_3}{Nu_4}\max(E,S)h_{sp}$ $h_{sp} = 0.023(Re_f)^{0.8}(Pr_f)^{0.4}\frac{k_f}{d_h},\ E = 0.6683Co^{-0.2}f(Fr_f) + 1058Bo^{0.7}$ $S = 1.136Co^{-0.9}f(Fr_f) + 667.2Bo^{0.7}$ $f(Fr_f) = 1(Fr_f \geqslant 0.04)$ or $f(Fr_f) = (25Fr_f)^{0.3}\ (Fr_f < 0.04)$	49.4
5	Liu and Winterton [33] (1991)	$h_{tp} = \frac{Nu_3}{Nu_4}\left((Eh_{sp})^2 + (Sh_{nb})^2\right)^{0.5}$ $h_{sp} = 0.023(Re_{fo})^{0.8}(Pr_f)^{0.4}\frac{k_f}{d_h},\ E = \left[1 + x_ePr_f\left(\frac{v_g}{v_f} - 1\right)\right]^{0.35},\ Re_{fo} = \frac{Gd_h}{\mu_f}$ $h_{nb} = 55P_r^{0.12}(-\log_{10}(P_r))^{-0.55}M_W^{-0.5}q''^{0.67}_{ch},\ S = (1 + 0.055E^{0.1}Re_{fo}^{0.16})^{-1}$ If $Fr_f \leqslant 0.05$, replace E by $EFr_f^{0.1-2Fr_f}$ and S by $SFr_f^{0.5}$, respectively	35.1

Table 4 (*continued*)

Correlation	Reference	Heat transfer coefficient, h_{tp}	MAE (%)
6	Steiner and Taborek [34] (1992)	$h_{tp} = \frac{Nu_3}{Nu_4}\left[(Eh_{sp})^3 + (Sh_{nb})^3\right]^{1/3}$ $h_{sp} = 0.023(Re_{fo})^{0.8}(Pr_f)^{0.4}\frac{k_f}{d_h},\ E = \left[(1-x_e)^{1.5} + 1.9x_e^{0.6}(v_g/v_f)^{0.35}\right]^{1.1}$ $h_{nb} = 25,581\ \mathrm{W/m^2\,K},\ S = F\left(\frac{q''_{ch}}{1.5\times10^5}\right)^{0.8-0.1\exp(1.75Pr)}\left(\frac{d_h}{0.01}\right)^{-0.4} f(M_W)$ $F = 2.816P_r^{0.45} + \left[3.4 + \frac{1.7}{1-P_r^7}\right]P_r^{3.7},\ f(M_W) = 0.72$	46.2
7	Lazarek and Black [7] (1982)	$h_{tp} = \frac{Nu_3}{Nu_4}\left[30(Re_{fo})^{0.857}(Bo)^{0.714}\frac{k_f}{d_h}\right]$	36.2
8	Tran et al. [11] (1996)	$h_{tp} = \frac{Nu_3}{Nu_4}\left[8.4\times10^5(Bo^2We_f)^{0.3}\left(\frac{v_g}{v_f}\right)^{-0.4}\right],\ We_f = \frac{v_f G^2 d_h}{\sigma}$	98.8
9	Lee and Lee [18] (2001)	$h_{tp} = \frac{Nu_3}{Nu_4}(Eh_{sp})$ $h_{sp} = Nu_4\frac{k_f}{d_h},\ E = 10.3\beta^{0.398}\ \phi_f^{0.598}$ $\phi_f = \left(1 + \frac{C}{X_{vt}} + \frac{1}{X_{vt}^2}\right)^{0.5},\ C = 6.185\times10^{-2}Re_{fo}^{0.726}$ $X_{vt} = \left(\frac{f_f}{f_g}\right)^{0.5}\left(\frac{1-x_e}{x_e}\right)\left(\frac{v_f}{v_g}\right)^{0.5},\ f_g = \frac{0.079}{Re_g^{0.25}},\ Re_g = \frac{Gx_e d_h}{\mu_g}$ $f_f = \frac{24}{Re_f}\left(1 - 1.355\beta + 1.947\beta^2 - 1.701\beta^3 + 0.956\beta^4 - 0.254\beta^5\right)$ $\beta = \frac{W_{ch}}{H_{ch}}$	272.1
10	Yu et al. [19] (2002)	$h_{tp} = \frac{Nu_3}{Nu_4}\left[6.4\times10^6(Bo^2We_f)^{0.24}\left(\frac{v_g}{v_f}\right)^{-0.2}\right]$	19.3
11	Warrier et al. [20] (2002)	$h_{tp} = \frac{Nu_3}{Nu_4}(Eh_{sp})$ $h_{sp} = Nu_4\frac{k_f}{d_h},\ E = 1.0 + 6Bo^{1/16} + f(Bo)x_e^{0.65}$ $f(Bo) = -5.3(1–855Bo)$	25.4

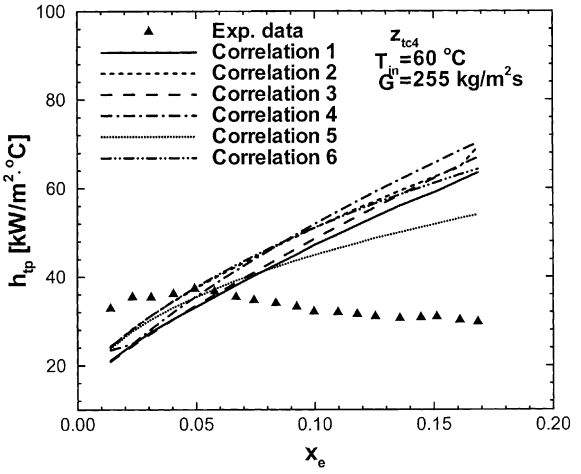

Fig. 7. Comparison of saturated flow boiling heat transfer coefficient data with macro-channel correlation predictions at z_{tc4} for $T_{in} = 60$ °C and $G = 255$ kg/m^2 s.

coefficient in flow developing regions of single-phase micro-channel heat sinks. As discussed above, the dominant flow pattern and heat transfer mechanism in water micro-channels are annular flow and forced convection boiling, respectively. Use of Eq. (10) in the present study to correct for three versus four-sided heating is justified by the fact that heat is transferred from the channel wall to the two-phase mixture first by single-phase convection to the liquid film. Additionally, the liquid film flow is mostly laminar because of the low water flow rate and small size of a micro-channel.

4.2. Macro-channel correlations

The first six correlations in Table 4 are based on flow boiling experimental data for macro-channels. Fig. 7 compares correlation predictions and experimental data at z_{tc4} as a function of thermodynamic equilibrium quality, x_e, for $T_{in} = 60$ °C and $G = 255$ kg/m^2 s. It is quite apparent that the trend predicted by all six correlations is drastically different from that of the present data. Most notably, the correlations predict an increasing h_{tp} with increasing x_e, while the data show the opposite trend. Furthermore, the correlations under-predict the data in the low x_e range, and over-predict it in the high x_e range.

The predictive capability of these correlations is further illustrated in Fig. 8(a) to (f) for all operating conditions of the present study. Aside from the deviations apparent in the variation of predicted-to-measured heat transfer coefficient ratio with x_e, these figures, as well as Table 4, include, for each correlation, the mean absolute error (MAE), defined as

$$\mathrm{MAE} = \frac{1}{M}\sum \frac{|h_{tp,pred} - h_{tp,exp}|}{h_{tp,exp}} \times 100\%, \quad (13)$$

where M is the number of data point. The mean absolute error of the macro-channel correlations ranges from 35.1% to 53.7%.

The discrepancy between the predictions of the six correlations and present data can be attributed to several factors. First, while these correlations are based on fairly sizeable experimental databases, the size of test tubes employed in their development is much larger than a micro-channel. As in most two-phase systems, extrapolating a correlation to operating conditions beyond those for which the correlation was originally developed can lead to appreciable error. A second reason for the discrepancy is these correlations are based on turbulent single-phase heat transfer correlations, such as the Dittus–Boelter correlation, in modeling the annular flow region since turbulent flow is prevalent in macro-channels. However, flow in a micro-channel is mostly laminar because of the small channel size and low flow rates used. For example, the inlet Reynolds number for the present tests ranged from 60 to 300.

4.3. Mini/micro-channel correlations

The last five correlations in Table 4 (correlations 7–11) are all based on saturated flow boiling heat transfer in mini/micro-channels. Comparisons between correlation predictions and the present data are shown in Figs. 9 and 10(a)–(e). Predictions of the correlations by Tran et al. (correlation 8) and Lee and Lee (correlation 9) have been excluded from Fig. 9 as the former predicts very small, and the latter very large values compared to the data. With a mean absolute error (MAE) of 36.2%, the performance of the Lazarek and Black correlation (correlation 7) is close to those of the macro-channel correlations. The correlation by Yu et al. (correlation 10) provides the best agreement (MAE of 19.3%) with the data among all eleven correlations tested. However, as shown in Figs. 9 and 10(d), this correlation does not capture the correct trend of heat transfer coefficient h_{tp} with x_e. On the other hand, the correlation by Warrier et al. (correlation 11), provides a closer prediction of the trend, but with a greater MAE of 25.4%.

It is important to emphasize that deviations from the experimental trends are not necessarily related to weaknesses in the correlations themselves, but more to the unique nature of flow boiling in micro-channels, and the operating conditions of water-cooled micro-channels falling outside the recommended application range for most correlations.

These findings clearly point to the need to develop new predictive tools that can both capture the correct trend of h_{tp} with x_e, and yield more accurate predictions. This is precisely the goal of part II of this study [21].

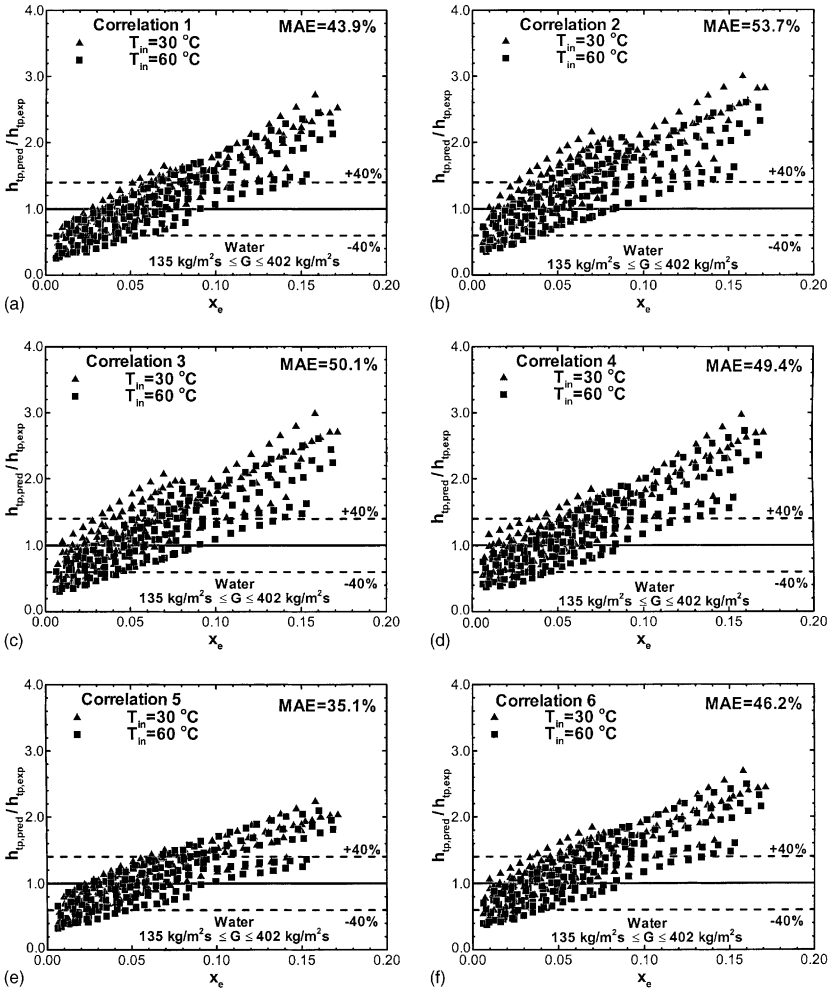

Fig. 8. Comparison of saturated flow boiling heat transfer coefficient data with predictions of macro-channel correlations of: (a) Chen [8,30]; (b) Shah [9,31]; (c) Gungor and Winterton [32]; (d) Kandlikar [15]; (e) Liu and Winterton [33] and (f) Steiner and Taborek [34].

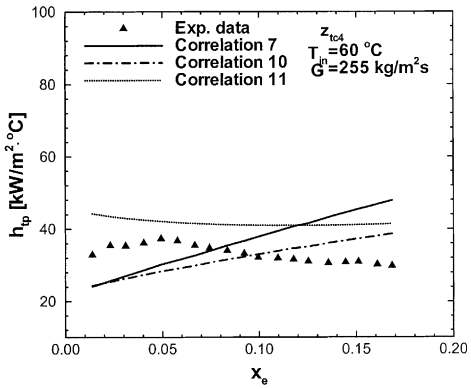

Fig. 9. Comparison of saturated flow boiling heat transfer coefficient data with mini/micro-channel correlation predictions at z_{tc4} for $T_{in} = 60$ °C and $G = 255$ kg/m^2 s.

5. Conclusions

This paper is part I of a two-part study devoted to flow boiling heat transfer of water in a two-phase micro-channel heat sink. In this paper, new experimental findings were discussed, complemented by identification of several unique features of flow boiling in a micro-channel, and assessment of the suitability of previous empirical heat transfer correlations to predicting the measured trends. Key findings from the study are as follows.

(1) The saturated flow boiling heat transfer coefficient in a water-cooled micro-channel heat sink is a strong function of mass velocity, and only a weak function of heat flux. This and prior studies by the authors point to annular flow as the dominant two-phase

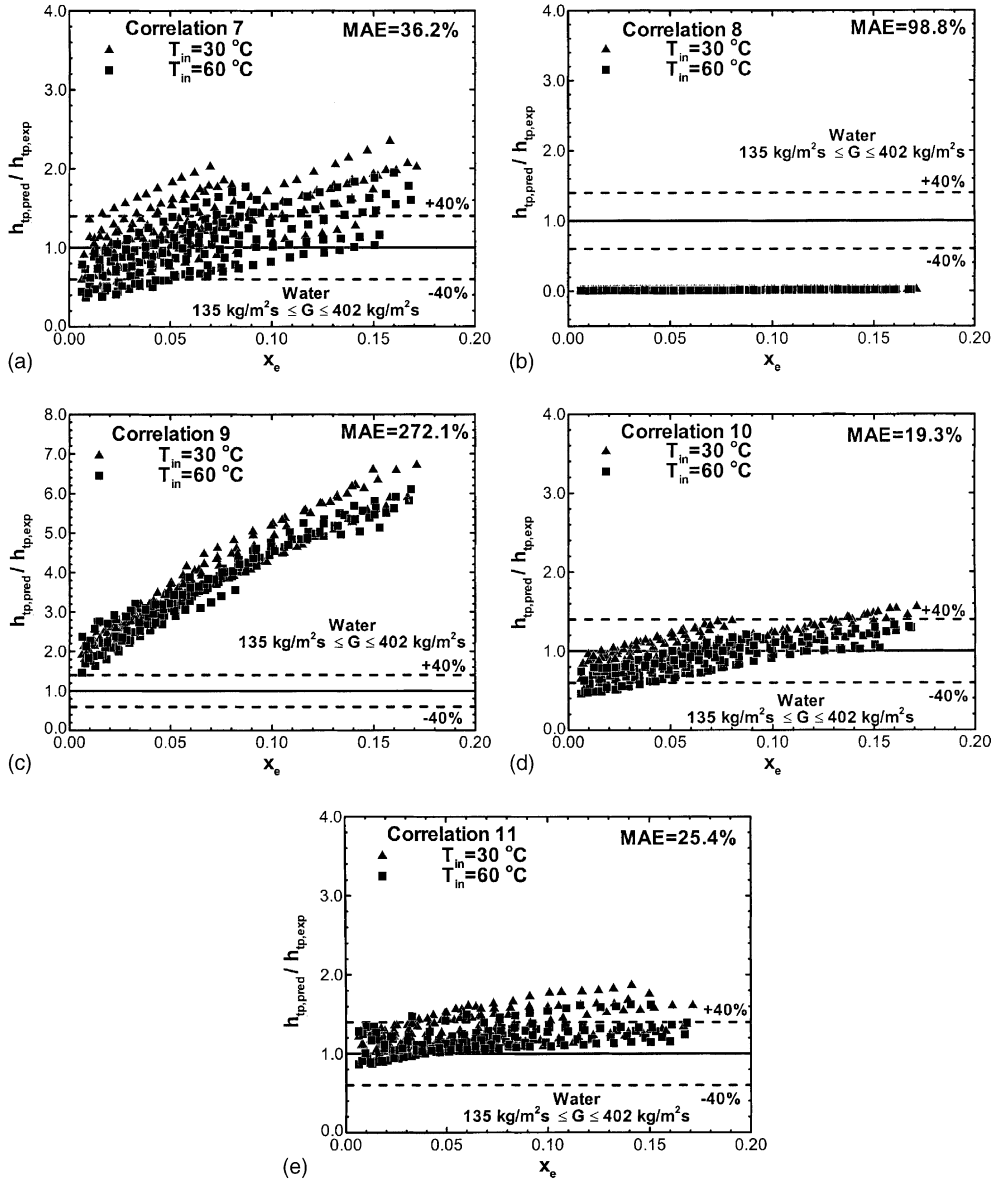

Fig. 10. Comparison of saturated flow boiling heat transfer coefficient data with predictions of mini/micro-channel correlations of: (a) Lazarek and Black [7]; (b) Tran et al. [11]; (c) Lee and Lee [18]; (d) Yu et al. [19] and (e) Warrier et al. [20]. Note different scale for Fig. 10(c).

flow pattern in micro-channels at moderate to high heat fluxes. These observations lend credence to the hypothesis that the dominant heat transfer mechanism for water micro-channel heat sinks is forced convective boiling and not nucleate boiling.

(2) The saturated flow boiling heat transfer coefficient decreases with increasing thermodynamic equilibrium quality. This trend is in sharp contradiction with that of macro-channels. This unique behavior is attributed to the strong influence of liquid droplet entrainment and deposition within the annular flow region.

(3) Predictions of six popular macro-channel heat transfer correlations and five correlations specifically developed for mini/micro-channels were compared to the present data. Significant deviations in overall trend point to a need for new predictive tools that can both capture the correct micro-channel heat transfer trends and yield more accurate predictions.

Acknowledgements

The authors are grateful for the support of the Office of Basic Energy Sciences of the US Department of Energy (Award no. DE-FG02-93ER14394 A7).

References

[1] M.B. Bowers, I. Mudawar, High flux boiling in low flow rate, low pressure drop mini-channel and micro-channel heat sinks, Int. J. Heat Mass Transfer 37 (1994) 321–332.
[2] M.B. Bowers, I. Mudawar, Two-phase electronic cooling using mini-channel and micro-channel heat sinks: part 1—design criteria and heat diffusion constraints, J. Electron. Packag. 116 (1994) 290–297.
[3] M.B. Bowers, I. Mudawar, Two-phase electronic cooling using mini-channel and micro-channel heat sinks: part 2—flow rate and pressure drop constraints, J. Electron. Packag. 116 (1994) 298–305.
[4] L. Zhang, J.M. Koo, L. Jiang, S.S. Banerjee, M. Ashegi, K.E. Goodson, J.G. Santiago, T.W. Kenny, Measurement and modeling of two-phase flow in microchannels with nearly-constant heat flux boundary conditions, in: A. Lee et al. (Eds.), Micro-Electro-Mechanical Systems (MEMS)—2000, ASME, Orlando, FL, 2000, MEMS-vol. 2, pp. 129–135.
[5] L. Jiang, M. Wong, Y. Zohar, Forced convection boiling in a microchannel heat sink, J. Microelectromech. Syst. 10 (2001) 80–87.
[6] G. Hetsroni, A. Mosyak, Z. Segal, G. Ziskind, A uniform temperature heat sink for cooling of electronic devices, Int. J. Heat Mass Transfer 45 (2002) 3275–3286.
[7] G.M. Lazarek, S.H. Black, Evaporative heat transfer, pressure drop and critical heat flux in a small vertical tube with R-113, Int. J. Heat Mass Transfer 25 (1982) 945–960.
[8] J.C. Chen, Correlation for boiling heat transfer to saturated fluids in convective flow, I&EC Process Design Develop. 5 (1966) 322–329.
[9] M.M. Shah, A new correlation for heat transfer during boiling flow through pipes, ASHRAE Trans. 82 (1976) 66–86.
[10] M.W. Wambsganss, D.M. France, J.A. Jendrzejczyk, T.N. Tran, Boiling heat transfer in a horizontal small-diameter tube, J. Heat Transfer 115 (1993) 963–972.
[11] T.N. Tran, M.W. Wambsganss, D.M. France, Small circular- and rectangular-channel boiling with two refrigerants, Int. J. Multiphase Flow 22 (1996) 485–498.
[12] P.A. Kew, K. Cornwell, Correlations for the prediction of boiling heat transfer in small-diameter channels, Appl. Therm. Eng. 17 (1997) 705–715.
[13] T.S. Ravigururajan, Impact of channel geometry on two-phase flow heat transfer characteristics of refrigerants in microchannel heat exchangers, J. Heat Transfer 120 (1998) 485–491.
[14] Y.Y. Yan, T.F. Lin, Evaporation heat transfer and pressure drop of refrigerant R-134a in a small pipe, Int. J. Heat Mass Transfer 41 (1998) 4183–4194.
[15] S.G. Kandlikar, A general correlation for saturated two-phase flow boiling heat transfer inside horizontal and vertical tubes, J. Heat Transfer 112 (1990) 219–228.
[16] Z.Y. Bao, D.F. Fletcher, B.S. Haynes, Flow boiling heat transfer of freon R11 and HCFC123 in narrow passages, Int. J. Heat Mass Transfer 43 (2000) 3347–3358.
[17] M.G. Cooper, Saturation nucleate pool boiling, a simple correlation, IChemE Symp. Ser. 86 (1984) 785–793.
[18] H.J. Lee, S.Y. Lee, Heat transfer correlation for boiling flows in small rectangular horizontal channels with low aspect ratios, Int. J. Multiphase Flow 27 (2001) 2043–2062.
[19] W. Yu, D.M. France, M.W. Wambsganss, J.R. Hull, Two-phase pressure drop, boiling heat transfer, and critical heat flux to water in a small-diameter horizontal tube, Int. J. Multiphase Flow 28 (2002) 927–941.
[20] G.R. Warrier, V.K. Dhir, L.A. Momoda, Heat transfer and pressure drop in narrow rectangular channel, Exp. Therm. Fluid Sci. 26 (2002) 53–64.
[21] W. Qu, I. Mudawar, Flow boiling heat transfer in two-phase micro-channel heat sinks—II. Annular two-phase flow model, Int. J. Heat Mass Transfer, doi:10.1016/S0017-9310(03)00042-5.
[22] W. Qu, I. Mudawar, Experimental and numerical study of pressure drop and heat transfer in a single-phase micro-channel heat sink, Int. J. Heat Mass Transfer 45 (2002) 2549–2565.
[23] W. Qu, I. Mudawar, Transport phenomena in two-phase micro-channel heat sinks, J. Electron. Packag. (in review).
[24] J.M. Robertson, P.C. Lovegrove, Boiling heat transfer with freon 11 (R11) in brazed aluminum' plate–fin heat exchangers, J. Heat Transfer 105 (1983) 605–610.
[25] V.P. Carey, G.D. Mandrusiak, Annular film-flow boiling of liquid in a partially heated, vertical channel with offset strip fins, Int. J. Heat Mass Transfer 29 (1986) 927–939.
[26] G.D. Mandrusiak, V.P. Carey, X. Xu, A experimental study of convective boiling in a partially heated horizontal channel with offset strip fins, J. Heat Transfer 110 (1988) 229–236.
[27] W. Qu, I. Mudawar, Thermal design methodology for high-heat-flux single-phase and two-phase micro-channel heat sinks, in: C.H. Amon et al. (Eds.), Proceedings of the Eighth Intersociety Conference on Thermal and Thermomechanical Phenomena in Electronic Systems (ITherm 2002), IEEE, San Diego, CA, 2002, pp. 347–359.
[28] J.G. Collier, J.R. Thome, Convective Boiling and Condensation, third ed., Oxford University Press, Oxford, 1994.
[29] S. Mukherjee, I. Mudawar, Pumpless loop for narrow channel and micro-channel boiling, J. Electron. Packag., in press.
[30] S. Edelstein, A.J. Perez, J.C. Chen, Analytic representation of convective boiling functions, AIChE J. 30 (1984) 840–841.
[31] M.M. Shah, Chart correlation for saturated boiling heat transfer: equations and further study, ASHRAE Trans. 88 (1982) 185–196.
[32] K.E. Gungor, R.H.S. Winterton, A general correlation for flow boiling in tubes and annuli, Int. J. Heat Mass Transfer 29 (1986) 351–358.
[33] Z. Liu, R.H.S. Winterton, A general correlation for saturated and subcooled flow boiling in tubes and annuli, based on a nucleate pool boiling equation, Int. J. Heat Mass Transfer 34 (1991) 2759–2766.
[34] D. Steiner, J. Taborek, Flow boiling heat transfer in vertical tubes correlated by an asymptotic model, Heat Transfer Eng. 13 (1992) 43–69.

[35] R.K. Shah, A.L. London, Laminar Flow Forced Convection in Ducts: a Source Book for Compact Heat Exchanger Analytical Data, Supl. 1, Academic Press, New York, 1978.

[36] H.H. Bau, Optimization of conduits' shape in micro-heat exchangers, Int. J. Heat Mass Transfer 41 (1998) 2717–2723.

[37] R.J. Phillips, Advances in thermal modeling of electronic components, in: A. Bar-Cohen, A.D. Kraus (Eds.), Microchannel Heat Sinks, vol. 2, 1990, pp. 109–184.

[38] S.F. Choquette, M. Faghri, M. Charmchi, Y. Asako, Optimum design of microchannel heat sinks, in: Micro-Electro-Mechanical Systems (MEMS), DSC-vol. 59, ASME, 1996, pp. 115–126.